Peak effect and dynamics of stripe- and pattern-forming systems on a periodic one-dimensional substrate

C. Reichhardt and C. J. O. Reichhardt

Theoretical Division and Center for Nonlinear Studies, Los Alamos National Laboratory, Los Alamos, New Mexico 87545, USA

We examine the ordering, pinning, and dynamics of two-dimensional pattern-forming systems interacting with a periodic one-dimensional substrate. In the absence of the substrate, particles with competing long-range repulsion and short-range attraction form anisotropic crystal, stripe, and bubble states. When the system is tuned across the stripe transition in the presence of a substrate, we find that there is a peak effect in the critical depinning force when the stripes align and become commensurate with the substrate. Under an applied drive, the anisotropic crystal and stripe states can exhibit soliton depinning and plastic flow. When the stripes depin plastically, they dynamically reorder into a moving stripe state that is perpendicular to the substrate trough direction. We also find that when the substrate spacing is smaller than the widths of the bubbles or stripes, the system forms pinned stripe states that are perpendicular to the substrate trough direction. The system exhibits multiple reentrant pinning effects as a function of increasing attraction, with the anisotropic crystal and large bubble states experiencing weak pinning but the stripe and smaller bubble states showing stronger pinning. We map out the different dynamic phases as a function of filling, the strength of the attractive interaction term, the substrate strength, and the drive, and demonstrate that the different phases produce identifiable features in the transport curves and particle orderings.

I. INTRODUCTION

Particle systems with competing long-range repulsive and short-range attractive interactions form a variety of patterned states, including crystals, stripes, bubbles, and void lattices [1–12]. For a fixed repulsion strength but increasing attraction strength, these systems form a crystal, then an anisotropic crystal, and finally stripe and bubble phases [9]. For fixed interaction strength but increasing particle densities, first bubbles, then stripes, then void lattices, and then a uniform crystal appear [9]. Similar patterns can arise even for systems with purely repulsive interactions if the interaction potential involves multiple length scales [13–15]. Pattern formation can occur in soft-matter systems such as colloidal assemblies, emulsions, and binary fluids [14–16], and in hard condensed-matter systems that include electron liquid crystals [17–24], composite fermion states [25], multiple component superconducting vortex systems [26–30], skyrmion systems [31], and various types of charge ordered states [32–36]. When pattern-forming systems couple to quenched disorder, they can exhibit pinned phases as well as depinning transitions and sliding phases under an applied drive [3,19,22–24,30,37–41]. If the quenched disorder is strong, then a glassy or structurally disordered state forms that depins plastically, and for high drives the system can dynamically reorder into patterned states such as moving stripes or moving bubbles [3,22,37,41]. The different dynamic states and transitions between them are associated with multiple steps in the transport curves [3,19,22,37,39], changes in the noise fluctuations [37,40–43], and modifications of the structure factors [30,37].

There have been extensive studies of systems of purely repulsive particles that form crystalline lattices under coupling to one- or two-dimensional periodic substrates [39,44–51]. Far less is known about how a pattern-forming system with competing interactions would behave when coupled to a periodic substrate. For particle systems with purely repulsive interactions, such as certain types of colloidal particles [44,49,51] and superconducting vortices [46,52–55], the relevant length scales are the average spacing between the particles and the periodicity of the substrate. In contrast, for stripe- or bubble-forming systems, additional length scales arise including the spacing between adjacent stripes or bubbles as well as the average spacing between the particles that compose each stripe or bubble, so a richer variety of commensuration effects are possible. Additionally, the mesoscale morphology in pattern-forming systems permits the appearance of matching or pinning effects that are not possible for repulsive point particles. For example, a stripe might show strong commensuration effects when interacting with a periodic one-dimensional (1D) substrate since the stripe can easily match the substrate shape. In general, if the attraction or repulsion strength or the filling fraction of the system is varied, then morphologies can emerge that are more strongly pinned due to better matching with the substrate length scales or shape, while for other morphologies, the patterns do not match, leading to changes in the pinning configurations, sliding, and transport.

In previous work on the static configurations of pattern-forming systems on a periodic 1D substrate, several new types of patterns were identified, such as modulated stripes and anisotropic bubbles [56]. Recently, we studied the depinning

of bubbles on periodic 1D substrates under a dc drive applied parallel to the substrate periodicity direction and found that the bubbles can depin either elastically or plastically depending on the substrate strength [57]. In addition, as the strength of the attractive interaction term increased, the bubbles became smaller and better pinned since they could fit within the substrate minima better than larger bubbles. When the bubbles depin elastically, there is a single peak in the differential velocity-force curves, while for plastic depinning, multiple peaks appear when the bubbles break up and move in various modes, such as via individual particles hopping from bubble to bubble or via a moving bubble shedding individual particles. At higher drives, the system can dynamically reorder back into a moving bubble lattice through a transition similar to the dynamic ordering found for superconducting vortices, colloidal particles, Wigner crystals, and skyrmions moving over random substrates [39,58–63].

In this work, we consider the pinning and dynamics of a pattern-forming system with competing long-range repulsion and short-range attraction interacting with a 1D periodic substrate as we sweep through parameters where crystal, stripe, and bubble states appear in a clean system. We find that the depinning threshold shows a peak or maximum in the stripe regime when the stripes form a commensurate state that aligns with the substrate troughs. When the substrate is strong, the stripes first depin plastically via the formation of running kinks or solitons, followed by the emergence of a disordered flowing state, while at high drives, there is a dynamical transition into a moving stripe phase where the stripes are wider and rotate with respect to the pinned configuration so that they are aligned with the driving direction. The anisotropic crystal state can also exhibit soliton depinning, disordered motion, and dynamical reordering into an anisotropic crystal at high drives. The drive needed to induce the reordering transition diverges near the boundary between the stripe and anisotropic crystal states. When the substrate lattice constant is decreased, the stripe and anisotropic crystal states remain strongly pinned, but the bubble phases show a pronounced depinning threshold decrease. For constant drives that are well above the depinning threshold, the average velocity passes through a dip in the stripe phase. When the substrate lattice constant is considerably smaller than the width of the stripes or bubbles, the system forms a pinned stripe or modulated stripe aligned perpendicular to the substrate trough direction that can depin into moving stripes or moving bubbles. When the particle-particle interaction strengths are held fixed while the filling fraction of the system is changed, we find that all three phases show steplike features in the depinning threshold that correlate with commensuration effects in which an integer number of rows of particles can fit inside an individual substrate trough. At high filling fractions, the stripes depin into a modulated solid that remains aligned with the substrate trough direction even at high drives. We also find that as the substrate strength increases, there is a sharp increase in the depinning threshold at the crossover from elastic to plastic depinning. For strong pinning at a fixed drive, the velocity is a nonmonotonic function of the magnitude of the attractive interaction term. The velocities are highest at zero attraction, pass through a minimum or reentrant pinning region in the stripe state, increase again for large bubbles, and then decrease

until a second reentrant pinning regime for small bubbles emerges.

II. SIMULATION

We consider a 2D system with periodic boundary conditions in the x and y directions. The sample contains N particles that have pairwise interactions composed of a long-range repulsive term, which favors formation of a uniform triangular lattice, and a competing short-range attractive term, which favors clump or bubble formation. In our system the repulsion dominates at very short distances, which prevents complete collapse of the particles to a point even for strong attractive interactions. The system is of size $L \times L$ with $L = 36$ and the particle density is $\rho = N/L^2$. The dynamics of particle i obey the following overdamped equation of motion:

$$\eta \frac{d\mathbf{R}_i}{dt} = -\sum_{j \neq i}^{N} \nabla V(R_{ij}) + \mathbf{F}_i^s + \mathbf{F}_D, \qquad (1)$$

where the damping term is set to $\eta = 1.0$. The first term on the right-hand side describes the particle-particle interactions, where

$$V(R_{ij}) = \frac{1}{R_{ij}} - B \exp(-\kappa R_{ij}). \qquad (2)$$

Here $R_{ij} = |\mathbf{R}_i - \mathbf{R}_j|$, and the location of particle $i(j)$ is $\mathbf{R}_{i(j)}$. For computational efficiency, we treat the long-range repulsive Coulomb interaction using a real-space Lekner summation technique as in previous work [3,56]. The short-range attraction term falls off exponentially with distance. The interaction potential of Eq. (2) produces crystal, stripe, bubble, or void lattice states depending on the values of ρ, the attractive force strength B, and the inverse screening length κ [3,4,9,37,56]. In this work we fix $\kappa = 1.0$. We focus on a particle density of $\rho = 0.44$ but also consider a range of densities from $\rho = 0.01$ to $\rho = 1.2$. For $\rho = 0.44$ in the absence of a substrate, the system forms a crystal for $B < 2.0$, a stripe state for $2.0 \leqslant B < 2.25$, and bubbles for $B \geqslant 2.25$.

The second term on the right-hand side of Eq. (2) represents the interaction with a 1D substrate that is sinusoidal in form with N_p minima and a lattice constant of $a_p = L/N_p$. Here

$$\mathbf{F}_s^i = F_p \cos(2\pi x_i/a_p)\hat{\mathbf{x}}, \qquad (3)$$

where x_i is the x position of particle i. We focus on substrates with $N_p = 8$ but also consider $N_p = 4$, 17, and 35. The particles are subjected to a uniform driving force $\mathbf{F}_D = F_D\hat{\mathbf{x}}$. The equations of motion are integrated via overdamped Brownian dynamics with a simulation time step of magnitude $dt = 0.0005$ in dimensionless simulation units.

The initial particle configuration is obtained through simulated annealing by placing the particles in a lattice configuration, subjecting them to a high temperature and then slowly cooling the system. The thermal forces are represented by Langevin kicks that appear as an additional term $\mathbf{F}^T$ in the equation of motion, with the properties $\langle F_i^T \rangle = 0$ and $\langle \mathbf{F}_i^T(t) \cdot \mathbf{F}_j^T(t') \rangle = 2\eta k_B T \delta_{ij}\delta(t - t')$, where k_B is Boltzmann's constant. The annealing procedure starts at a temperature of $F^T = 5$ and lasts between 2×10^6 and 5×10^6 simulation

time steps. The longer annealing times were necessary near the transition between stripe and bubble or lattice states. We tested to ensure that annealing over even longer intervals does not produce significantly different states. After the simulated annealing is complete, the temperature is set to zero. After initialization, we apply a driving force to all of the particles. We typically wait 10^4 or more simulation time steps after changing the driving force to avoid any transient effects, and then we measure the time-averaged particle velocity in the driving direction, $\langle V \rangle = \sum_i^N \mathbf{v}_i \cdot \hat{\mathbf{x}}$, where we perform the time average during 6×10^5 simulation time steps for each value of the driving current. From this measure we can construct a velocity-force curve.

Our selection of system size, particle densities, and interaction potential parameters is based on our knowledge from previous work [9] of regimes that produce crystal, stripe, and bubble phases in the absence of a substrate as B is varied over the range $0 < B < 5.0$. This permits us to study the dynamics of all three phases. We varied the substrate spacings to include cases where the width of the bubbles or stripes is less than, comparable to, or greater than the substrate spacing in order to explore the most important size ratio regimes. The range of drives we selected extends from well below to well above the maximum pinning force in order to cover the full range of possible sliding phases.

III. RESULTS

In Fig. 1, we show the pinned particle configurations at $F_D = 0$ for a system with $\rho = 0.44$, $N_p = 8$, and $F_p = 1.0$. At $B = 0.2$, in the absence of a substrate a uniform crystal would form, but as illustrated in Fig. 1(a), the presence of a substrate produces an anisotropic crystal that has small density modulations induced by the substrate potential. Figure 1(b) shows a stripe phase at $B = 2.15$, where the stripes are aligned with the substrate troughs and each trough contains two rows of particles. At $B = 2.75$, the bubble phase shown in Fig. 1(c) forms. In Fig. 1(d), the stripe state with $B = 2.15$ from Fig. 1(b) is placed on a substrate with $N_p = 17$, which reduces the substrate lattice constant. Here each substrate trough captures a single row of particles.

We next examine the driving force F_c at which the system depins as a function of B for the system in Figs. 1(a)–1(c) with $\rho = 0.44$, $F_p = 1.0$, and $N_p = 8$ by performing a series of simulations and constructing velocity-force curves. In Fig. 2(a), we plot F_c for a range of B values that span a pinned isotropic crystal (PAC) state, a pinned stripe (PS) state, and a pinned bubble (PB) state. For small B, the depinning threshold has a low value of $F_c = 0.05$, indicating that the anisotropic crystal phases are weakly pinned. As B increases, F_c increases and reaches a peak value of $F_c = 0.75$ in the stripe phase, showing that the stripes are strongly pinned. For B values above the peak in F_c, the stripes become nonuniform and develop wider patches separated by narrower patches as the system begins to destabilize toward the bubble state. In this patchy regime of the stripe state, the depinning threshold decreases with increasing B because the wider portions of the stripe are less well pinned than the narrower portions of the stripe, lowering the overall depinning threshold. When B becomes sufficiently large, the system enters the bubble phase,
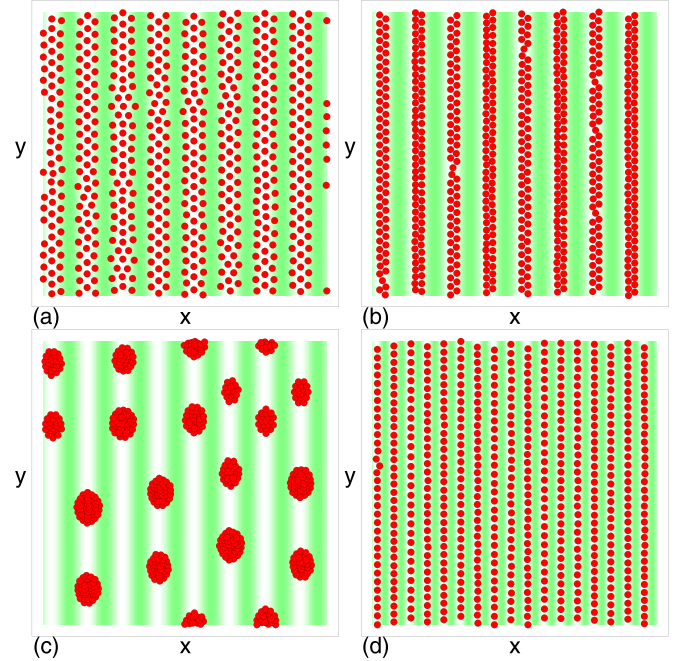

FIG. 1. [(a)–(c)] Particle positions (red circles) and substrate potential (green shading) for a sample with particle density $\rho = 0.44$, pinning strength $F_p = 1.0$, and number of substrate minima $N_p = 8$ in the absence of driving, $F_D = 0$, for different attractive interaction strengths B. Note that here and throughout this work, the size of the circles representing the particles is chosen purely for visual convenience; the particles do not have a defined outer edge. (a) An anisotropic crystal at $B = 0.2$. (b) A stripe state at $B = 2.15$. (c) A bubble phase at $B = 2.75$. (d) The $B = 2.15$ system from panel (b) with a higher number of substrate minima, $N_p = 17$, where each stripe is composed of a single row of particles.

where a local minimum of $F_c = 0.39$ appears at $B = 2.9$. As B increases further, the bubbles shrink in size and the depinning threshold increases again since the smaller bubbles fit better into the pinning troughs, as shown in a previous study [57]. In Fig. 2(b) we plot the average velocity $\langle V \rangle$ versus B at a constant drive of $F_D = 1.0$. In the absence of a substrate, $\langle V \rangle = F_D = 1.0$ for this value of F_D. In the presence of the substrate, $\langle V \rangle$ decreases with increasing B until it reaches a local minimum in the stripe phase. The velocity then increases with increasing B up to a local maximum value that appears early in the bubble phase and finally decreases again with increasing B for large B. If the same measurement is performed at larger values of F_D, then we find that the dip in $\langle V \rangle$ in the stripe phase persists but becomes flatter with increasing F_D. This dip is a signature of the peak in the the critical depinning force that appears when the system has formed an anisotropic stripe state.

Obtaining a reduced set of parameters that can describe the behavior of F_c versus B is nontrivial since this is a many-body system with complex interactions. We can, however, treat two limiting cases in which the behavior is close to the single particle limit so that the depinning force approaches the maximum pinning force from the substrate. The first case is in the stripe state where the stripes are aligned with the substrate. Here $F_c/F_p = 0.8$, a value that is less than 1.0 due to the fact
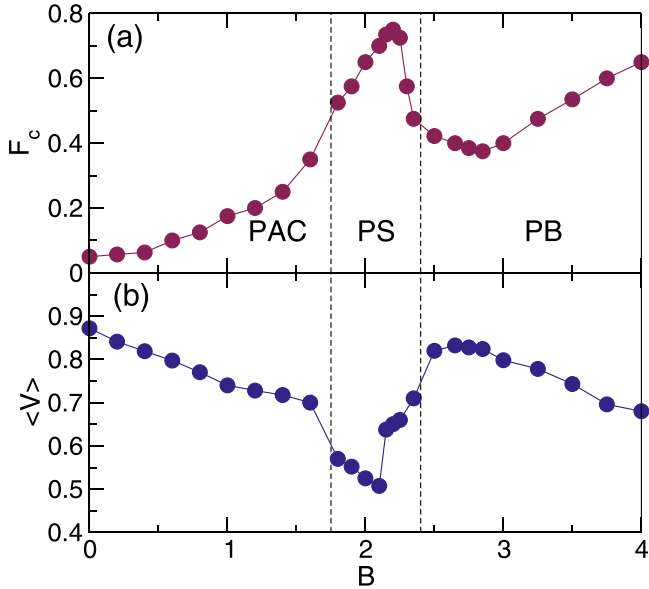
FIG. 2. (a) The critical depinning force F_c vs B for the system from Figs. 1(a)–1(c) with $\rho = 0.44$, $F_p = 1.0$, and $N_p = 8$. (b) The average velocity per particle $\langle V \rangle$ vs B at fixed $F_D = 1.0$. The dashed lines indicate that the system forms a pinned anisotropic crystal (PAC) for $B < 1.75$, a pinned stripe (PS) state for $1.75 \leqslant B \leqslant 2.25$, and a pinned bubble (PB) state for $B > 2.25$. In the PS state, there is a peak in the depinning force and a dip in the velocity.

that the finite width of the stripes prevents all of the particles from sitting at the very bottom of the substrate potential. The second case is in the bubble state at large B where the bubbles become so small that they act nearly like a low density of single particles; however, the finite width of the bubbles compared to actual single particles again suppresses the value of F_c/F_p below 1.0. For $B = 0.0$, the system becomes identical to that studied in previous simulations of repulsive particles on a periodic 1D substrate [52,54]; however, since the parameters we consider here do not correspond to a commensurate state, the depinning threshold is relatively low.

In Fig. 3 we plot the velocity-force curves $\langle V \rangle$ versus F_D along with the corresponding differential velocity curves $d\langle V \rangle/dF_D$ versus F_D for the system in Fig. 2 with $\rho = 0.44$, $F_p = 1.0$, and $N_p = 8$ at $B = 2.75$ in the bubble phase and $B = 2.15$ in the stripe phase. For $B = 2.75$, the depinning threshold is low, there is a single peak in $d\langle V \rangle/dF_D$, and the differential velocity approaches $d\langle V \rangle/dF_D = 1.0$ just above this peak. Here the bubbles depin elastically and pass directly from a pinned bubble state to a moving bubble phase. At $B = 2.15$, the stripes depin plastically, and there is a double peak in the differential conductivity, with the initial depinning producing a peak near $F_D = 0.74$ followed by a second peak in $d\langle V \rangle/dF_D$ near $F_D = 0.925$. The differential velocity does not approach $d\langle V \rangle/dF_D = 1$ until $F_D > 1.3$. The initial depinning of the stripe state occurs via the sliding of kinks or solitons, where individual particles hop out of one well and displace a particle in the adjacent well. This is illustrated in Fig. 4(a) where we highlight the particle trajectories from the stripe state in Fig. 3 at $F_D = 0.825$, just above F_c. For drives of $0.95 < F_D < 1.2$, the stripe system forms the
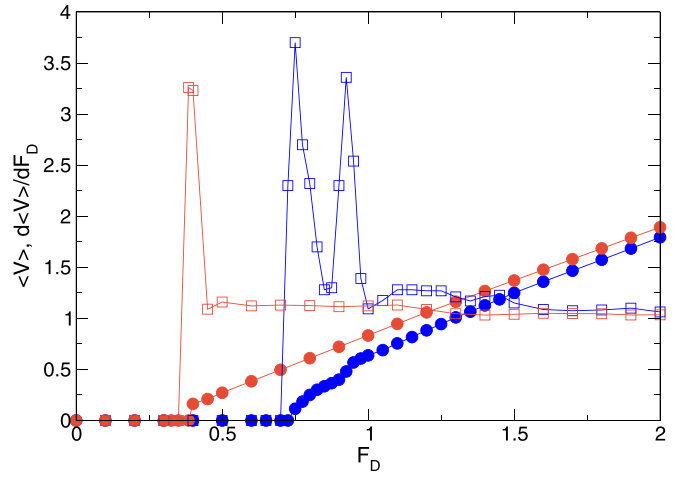

FIG. 3. The velocity-force curves $\langle V \rangle$ vs F_D (solid circles) and the corresponding differential velocity $d\langle V \rangle/dF_D$ vs F_D curves (open squares) for the system from Fig. 2 with $\rho = 0.44$, $F_p = 1.0$, and $N_p = 8$. At $B = 2.15$ (blue curves), the system is in the stripe state and there is a double peak in the differential velocity, while at $B = 2.75$ (red curves), the system is in the bubble state and there is a single peak in $d\langle V \rangle/dF_D$.

moving disordered structure shown in Fig. 4(b) at $F_D = 1.1$, while at $F_D = 1.5$, a moving stripe structure that is aligned with the driving direction and not the substrate trough direction appears, as illustrated in Fig. 4(c). Since the number of
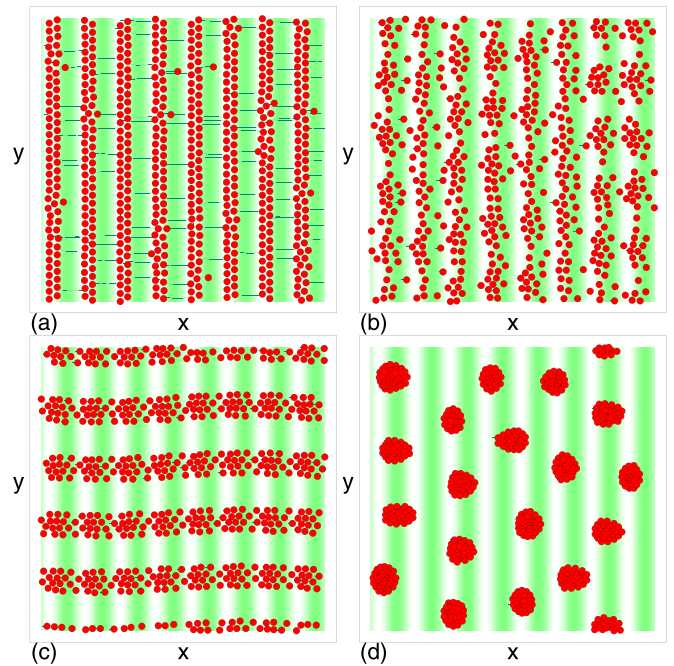

FIG. 4. Particle positions (red circles) and substrate potential (green shading) for the system from Fig. 3 with $\rho = 0.44$, $F_p = 1.0$, and $N_p = 8$. (a) The soliton flow phase at $B = 2.15$ and $F_D = 0.825$. Lines indicate the trajectories of individual particles. (b) A disordered moving phase at $B = 2.15$ and $F_D = 1.0$. (c) A moving stripe phase at $B = 2.15$ and $F_D = 1.5$. (d) A moving bubble phase at $B = 2.75$ and $F_D = 1.5$.
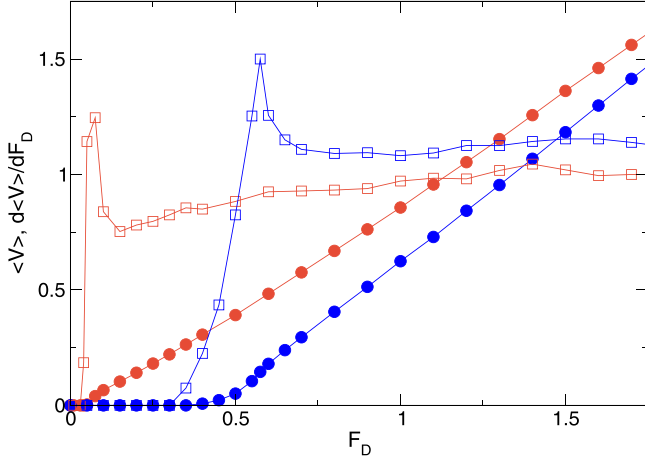
FIG. 5. $\langle V \rangle$ vs F_D (solid circles) and the corresponding $d\langle V \rangle/dF_D$ vs F_D (open squares) for the system from Fig. 2 with $\rho = 0.44$, $F_p = 1.0$, and $N_p = 8$ in the anisotropic crystal state at $B = 1.6$ (blue curves) and $B = 0.2$ (red curves).

stripes in the moving stripe structure is smaller than N_p, each stripe has a width of four particles. There is also a periodic density modulation along the length of the stripe. The moving bubble state that appears above depinning for the $B = 2.75$ system in Fig. 3 is illustrated in Fig. 4(d) at $F_D = 1.5$, where the bubbles have developed a slight anisotropy favoring the driving direction.

In Fig. 5, we show the $\langle V \rangle$ and $d\langle V \rangle/dF_D$ versus F_D curves for the system from Fig. 2 in the anisotropic crystal state at $B = 1.6$ and $B = 0.2$. When $B = 0.2$, the particles undergo weak plastic depinning from the anisotropic pinned crystal to a flowing disordered state and then transition near $F_D = 0.4$ into a dynamically reordered moving crystal. The corresponding $d\langle V \rangle/dF_D$ curve contains only a single peak at the depinning transition. At $B = 1.6$, the depinning is strongly plastic, and soliton-like flow occurs, corresponding to the nonlinear segment of the $\langle V \rangle$ versus F_D curve appearing below $F_D = 0.4$. As the drive increases, a disordered flow regime appears, followed by dynamical ordering into a moving crystal for $F_D > 0.65$. In Fig. 6(a) we show the particle positions
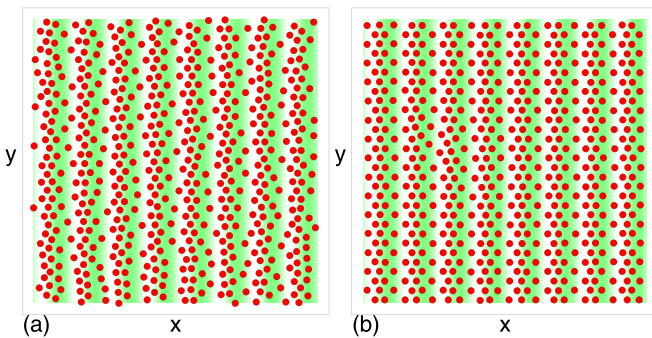

FIG. 6. Particle positions (red circles) and substrate potential (green shading) for the system from Fig. 5 with $\rho = 0.44$, $F_p = 1.0$, $N_p = 8$, and $B = 1.6$. (a) $F_D = 0.6$ in the partially disordered phase. (b) $F_D = 1.5$ in the dynamically reordered moving anisotropic crystal phase.
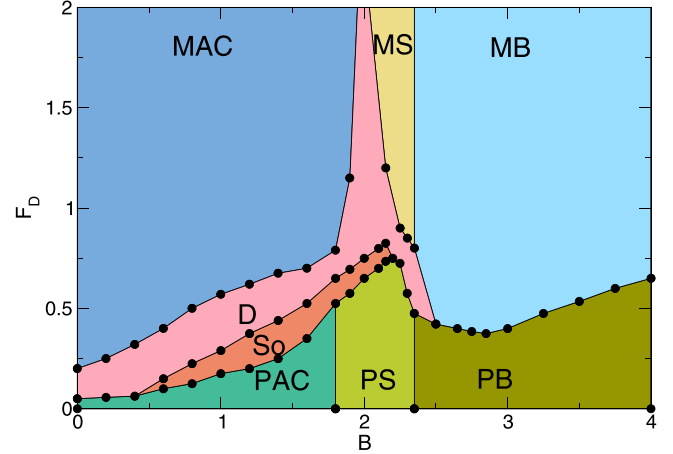

FIG. 7. Dynamic phase diagram as a function of F_D vs B constructed from the transport curves, pinned structures, and moving structures for the system from Fig. 2 with $\rho = 0.44$, $N_p = 8$, and $F_p = 1.0$. There are three pinned phases: pinned anisotropic crystal (PAC), pinned stripe (PS), and pinned bubble (PB). The moving phases are soliton flow (So), disordered flow (D), moving anisotropic crystal (MAC), moving stripe (MS), and moving bubble (MB).

in the disordered flowing state at $B = 1.6$ and $F_D = 0.6$, and in Fig. 6(b) we illustrate the dynamically reordered moving anisotropic lattice at $F_D = 1.5$. The lattice displays a small density modulation from the substrate.

From the features in the transport curves and the particle arrangements, we can construct a dynamic phase diagram of the different phases as a function of F_D versus B for the sample with $\rho = 0.44$, $N_p = 8$, and $F_p = 1.0$, as shown in Fig. 7. The pinned states consist of the PAC, PS, and PB phases. The PS can depin into either a moving soliton (So) phase or a disordered (D) plastic flow phase, and it dynamically reorders into a moving stripe (MS) at high drives. The PB phase shows a region of plastic depinning near $B = 2.35$, but for larger B it elastically depins directly into the moving bubble (MB) phase. The PAC depins into the So phase and then transitions into the D phase before undergoing dynamic reordering into a moving anisotropic crystal (MAC). At small B, there is no soliton depinning and the PAC depins directly into D flow. An interesting feature is that the drive needed to transition to the moving stripe phase diverges near the MAC-MS boundary. It is likely that the energy difference between the moving anisotropic crystal and the moving stripe state is small near this boundary, so the competition between the two phases causes a disordered flow to emerge. Only at very high drives is it possible to resolve the energy difference between the MAC and MS state and escape from the disordered flow at the MAC-MS boundary. In general, we identify the different phases using direct imaging combined with the changes in the transport curves and in the differential resistivity. Other image-based measures are also possible, such as obtaining the average distance to the closest neighbor of each particle, a measure that exhibits sharp changes at the transitions between different phases in the absence of a substrate [9].
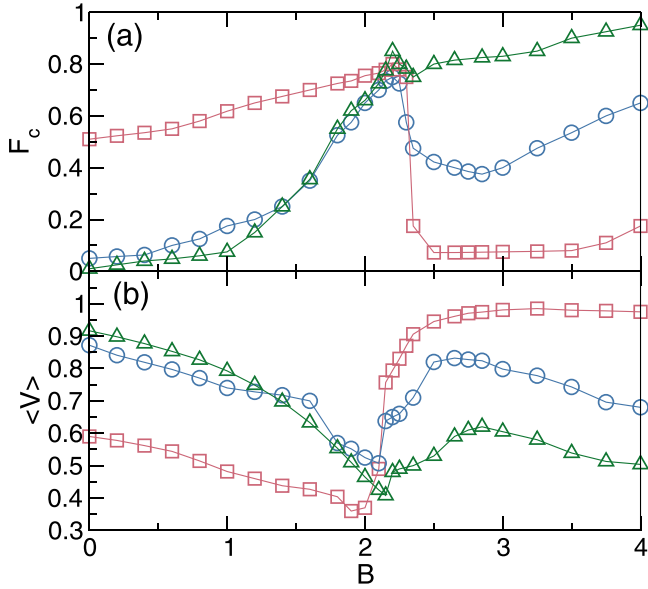
FIG. 8. (a) The depinning threshold F_c vs B in samples with $\rho = 0.44$ and $F_p = 1.0$ at $N_p = 4$ ($a_p = 9.0$, green), $N_p = 8$ ($a_p = 4.5$, blue), and $N_p = 17$ ($a_p = 2.1$, pink). There is a maximum in F_c in the stripe phase. (b) The corresponding velocity $\langle V \rangle$ vs B at $F_D = 1.0$ has a dip in the stripe regime.

IV. CHANGING THE SUBSTRATE PERIODICITY

We next fix the particle density while changing the number N_p of substrate minima, which alters the substrate lattice constant a_p. In Fig. 8(a) we plot F_c versus B in samples with $\rho = 0.44$ and $F_p = 1.0$ at $N_p = 4$ ($a_p = 9.0$), $N_p = 8$ ($a_p = 4.5$), and $N_p = 17$ ($a_p = 2.1$). The $N_p = 8$ curve was already highlighted in Fig. 2. For $N_p = 4$, the anisotropic crystal phase becomes even more weakly pinned since the particles are able to fill all of the space; however, the bubble phase is now strongly pinned since the bubbles can easily fit within the substrate troughs. A small peak in F_c appears near the stripe phase. When $N_p = 17$, the anisotropic crystal is strongly pinned, and the pinned stripe configuration at $B = 2.15$, illustrated in Fig. 1(d), consists of rows that are a single particle wide. The bubble phase for $N_p = 17$ is weakly pinned because an individual bubble has a radius that is much larger than the pinning period of $a_p = 2.1$. Figure 8(b) shows the corresponding $\langle V \rangle$ versus B curves at $F_D = 1.0$, where a local minimum in $\langle V \rangle$ appears in the stripe phase. For $N_p = 17$, the bubbles at higher values of B slide at nearly the expected free flow velocity of $\langle V \rangle = 1.0$.

In Fig. 9(a), we show the pinned particle configuration for the bubble phase from Fig. 8 at $B = 2.75$ and $N_p = 17$. The bubble radius is twice as large as the substrate spacing, so the bubbles can slide easily over the substrate. Figure 9(b) shows the same system at $N_p = 4$, where the bubbles easily fit within the substrate troughs and are strongly pinned. At $B = 0.2$ and $N_p = 4$ in Fig. 9(c), the system forms a density modulated crystal that is weakly pinned since some of the particles are located near maxima of the substrate potential. In Fig. 9(d), the particle configuration at $B = 0.2$ and $N_p = 17$ is an anisotropic crystal with stripelike pattern that is almost the same as the configuration found in Fig. 2 for $B = 2.15$ and the
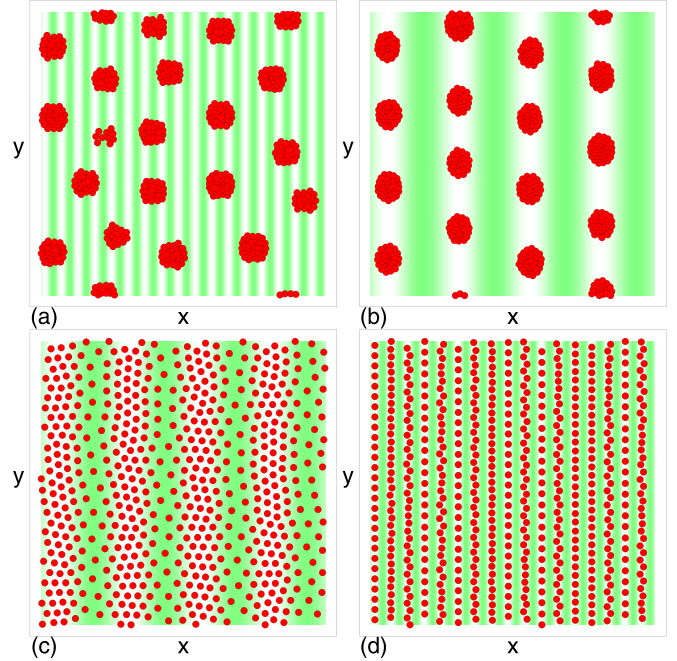

FIG. 9. Particle positions (red circles) and substrate potential (green shading) for the system from Fig. 8 with $\rho = 0.44$ and $F_p = 1.0$ in the pinned state. (a) Weakly pinned bubbles at $B = 2.75$ and $N_p = 17$. (b) Strongly pinned bubbles at $B = 2.75$ and $N_p = 4$. (c) A weakly pinned anisotropic crystal at $B = 0.2$ and $N_p = 4$. (d) A strongly pinned anisotropic crystal structure at $B = 0.2$ and $N_p = 17$.

same substrate spacing. In this case, for $B = 0.2$, the substrate free system forms a crystal; however, the spacing of the substrate is small enough that the particles form a chainlike state. Figure 8(a) shows that the depinning threshold remains nearly constant for the anisotropic crystal and stripe states over the range $0 < B < 2.25$ and only drops in the bubble phase when $B \geqslant 2.25$.

For $N_p = 17$, we observe dynamical phases similar to those described above for the $N_p = 8$ system. There are, however, some differences in the transport curves, as shown in Fig. 10(a) where we plot $\langle V \rangle$ versus F_D at $B = 1.0$, 2.15, and 2.75. When $B = 2.15$, there is a two-step depinning process from a soliton like flow to a moving stripe state. The second depinning transition is more discontinuous than the first, resulting in the appearance in Fig. 10(b) of a strong peak in $d\langle V \rangle / dF_D$ versus F_D at the onset of the stripe phase. For $B = 1.0$, there is also a two-step depinning process that produces a double peak in $d\langle V \rangle / dF_D$, but neither of the peaks are as sharp as the peak found in the $B = 2.15$ sample. At $B = 2.75$, there is a single peak in $d\langle V \rangle / dF_D$, and the pinned bubble phase depins elastically to a moving bubble phase. Another interesting feature is that even though the depinning threshold is largest for $B = 2.15$, the $B = 1.0$ and $B = 2.15$ velocity-force curves cross at higher drives so that, within the moving stripe regime, the velocity is higher for $B = 2.15$ than for $B = 1.0$, indicating that for this value of N_p the stripes can flow with less resistance than the moving anisotropic crystal. In Fig. 11(a), we illustrate the moving stripe state for the system from Fig. 10 with $N_p = 17$ at $B = 2.15$ and $F_D = 1.2$, where the stripes are aligned with the driving direction and
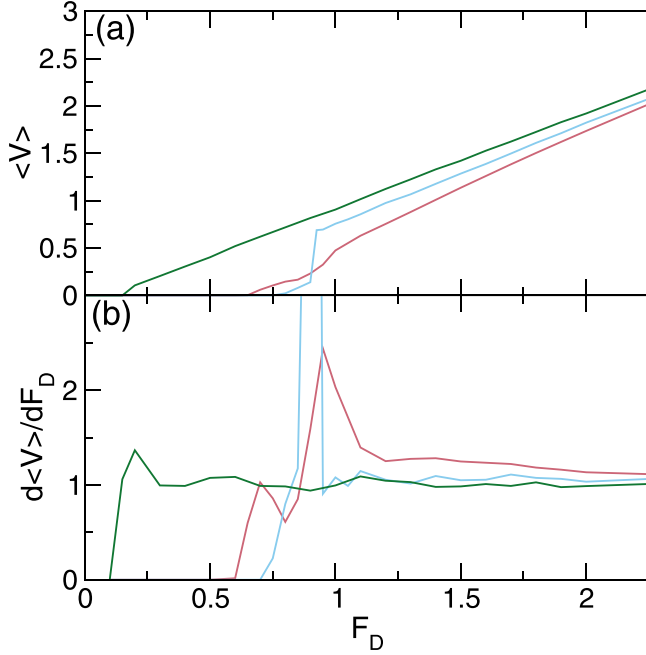
FIG. 10. (a) $\langle V \rangle$ vs F_D for a system with $N_p = 17$, $\rho = 0.44$, and $F_p = 1.0$ at $B = 1.0$ (red), 2.15 (blue), and 2.75 (green). (b) The corresponding $d\langle V \rangle / dF_D$ vs F_D curves.
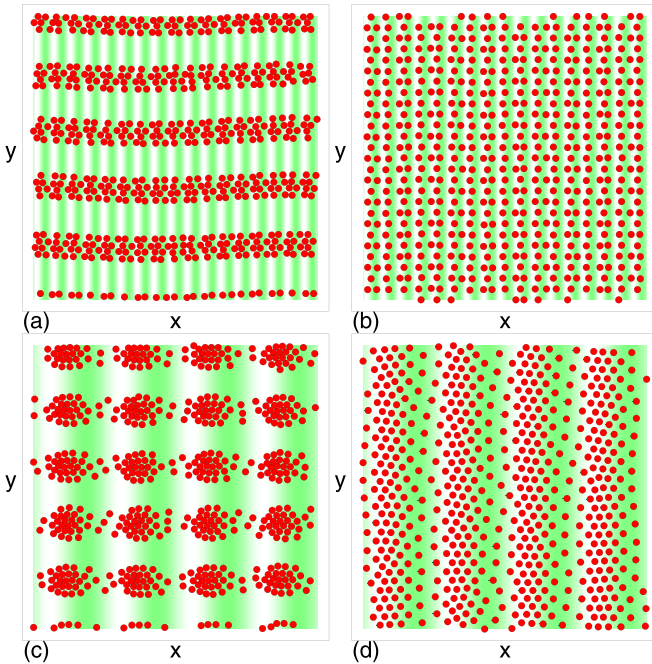

FIG. 11. Particle positions (red circles) and substrate potential (green shading) for the system from Fig. 10 with $\rho = 0.44$, $F_p = 1.0$, and $F_D = 1.2$ for varied B and N_p. (a) The moving stripe state at $N_p = 17$ and $B = 2.15$. (b) The moving crystal phase at $N_p = 17$ and $B = 1.0$. (c) The moving stripe state at $N_p = 4$ and $B = 2.15$, where the stripes are more bubblelike. (d) The moving modulated solid at $N_p = 4$ and $B = 1.0$.
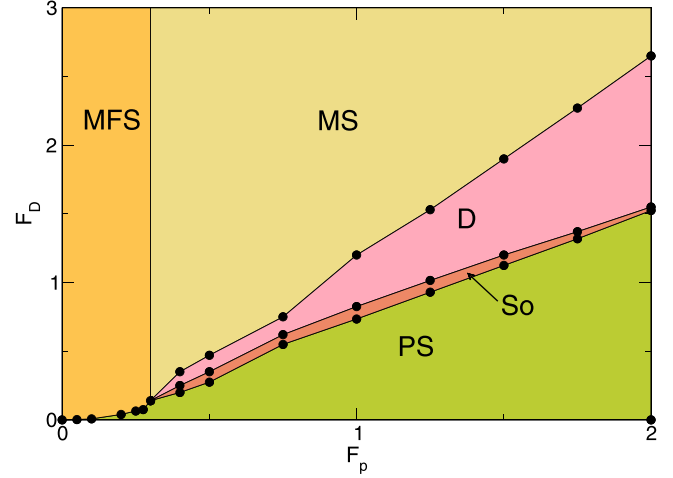

FIG. 12. Dynamic phase diagram as a function of F_D vs F_p for a stripe-forming system at $\rho = 0.44$, $B = 2.15$, and $N_p = 8$ showing the pinned stripe (PS), soliton flow (So), disordered flow (D), moving stripe (MS), and moving floating solid (MFS). For $F_p \leqslant 0.35$, the PS depins elastically to a MFS. For $F_p > 0.35$ the PS depins plastically to the So state, then transitions into a D phase and finally a MS state.

are four particles wide. Figure 11(b) shows the moving crystal phase at $B = 1.0$ and $F_D = 1.2$. When $N_p = 4$, a similar set of phases occurs but the features in the transport curves are not as sharp. In Fig. 11(c) we show the $N_p = 4$ stripe phase at $B = 2.15$ and $F_D = 1.2$, where the stripes are more bubblelike. Figure 11(d) shows the modulated moving solid at $B = 1.0$ and $F_D = 1.2$ in the $N_p = 4$ system.

V. EFFECT OF SUBSTRATE STRENGTH

In general, changing the substrate strength does not modify which dynamic phases are present, but it shifts the boundaries between the phases. As a function of increasing pinning strength, for the bubble phases we find a transition from elastic to plastic depinning at a critical pinning force that is accompanied by a noticeable increase in F_c [57]. For the anisotropic crystal, we observe a similar step up in F_c at an elastic to plastic depinning transition, but it is not as pronounced as in the bubble phases. In Fig. 12 we plot a dynamic phase diagram as a function of F_D versus F_p for the stripe state at $B = 2.15$, $\rho = 0.44$, and $N_p = 8$. For $F_p \leqslant 0.35$, the stripes depin elastically and do not rotate to align with the driving direction but instead enter what we term a moving floating solid state. For $F_p > 0.35$, the system depins plastically. There is a small jump up in the depinning threshold at the elastic-to-plastic depinning transition, and F_c increases linearly with increasing F_p in the plastic depinning regime. As the drive increases above the plastic depinning transition, the system first passes through a soliton flow phase and then into a disordered flow state before reaching a moving stripe state in which the stripes are aligned with the driving direction.

When $N_p = 17$, the transition from elastic to plastic depinning as a function of increasing F_p is much sharper than in the $N_p = 8$ system. In Fig. 13 we plot F_c versus F_p for a system with $\rho = 0.44$ and $N_p = 17$ at $B = 1.6$ in the anisotropic crystal state, $B = 2.15$ in the stripe state, and $B = 2.35$ in the
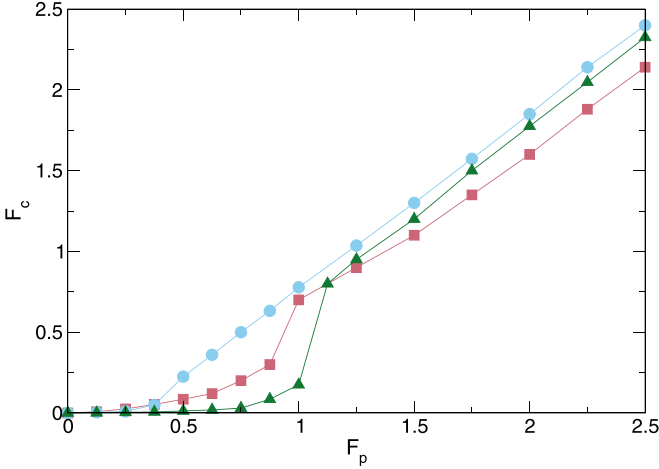
FIG. 13. F_c vs F_p for a system with $\rho = 0.44$ and $N_p = 17$ at $B = 1.6$ (anisotropic crystal, red squares), $B = 2.15$ (stripe, blue circles), and $B = 2.35$ (bubble, green triangles).

bubble state. The depinning threshold is largest for the stripe system at all F_p, and the stripe state undergoes an elastic-to-plastic depinning transition near $F_p = 0.35$. For $B = 2.35$, the bubbles depin elastically up to $F_p = 1.0$, and then a large increase in the depinning threshold occurs at the transition to plastic depinning. For $B = 1.6$, the transition from elastic to plastic depinning appears at $F_p = 0.9$ and is accompanied by a large increase in F_c. Within the plastic depinning regime, the depinning threshold increases linearly with increasing F_p as is found for other interacting particle systems [39], while in the elastic depinning regime, F_c is a nonlinear function of F_p. Our results are not accurate enough to give the exact fitting function, but systems that depin elastically often have a depinning threshold that increases quadratically with increasing pinning force [39].

When $B > 2.0$, another effect we observe is that for stronger substrates and higher N_p, the system forms pinned stripes or modulated stripes that are perpendicular to the substrate troughs. In Fig. 14(a), we illustrate the pinned configuration for a system with $N_p = 35$, $F_p = 2.5$, and $B = 1.6$, where a distorted crystal state appears. Figure 14(b) shows the same system at $B = 2.15$, where a pinned stripe appears that is aligned in the x direction, perpendicular to the substrate troughs. At $N_p = 17$, $F_p = 3.0$, and $B = 2.75$ in Fig. 14(c), we find a more discontinuous modulated stripelike pattern aligned with the x direction, while a stripelike pinned pattern appears for $N_p = 35$, $F_p = 1.5$, and $B = 2.75$ in Fig. 14(d). For either value of N_p, when $B = 2.15$, the system can still depin plastically via solitons that run along the stripe, but as the drive increases, the entire stripe structure depins and remains aligned in the direction of the drive. For $B = 2.75$, the moving state forms bubbles, and depinning occurs via the formation of a bubble along the modulated stripe that picks up particles as it travels along the stripe as if the stripe is providing a track for motion. In Fig. 15 we illustrate the time evolution of the depinning of the stripe state into a moving bubble state for a sample with $F_p = 3.0$, $B = 2.75$, $N_p = 35$, $\rho = 0.44$, and $F_D = 2.0$. At early times in Fig. 15(a), the depinning occurs via the formation of bubbles that move along
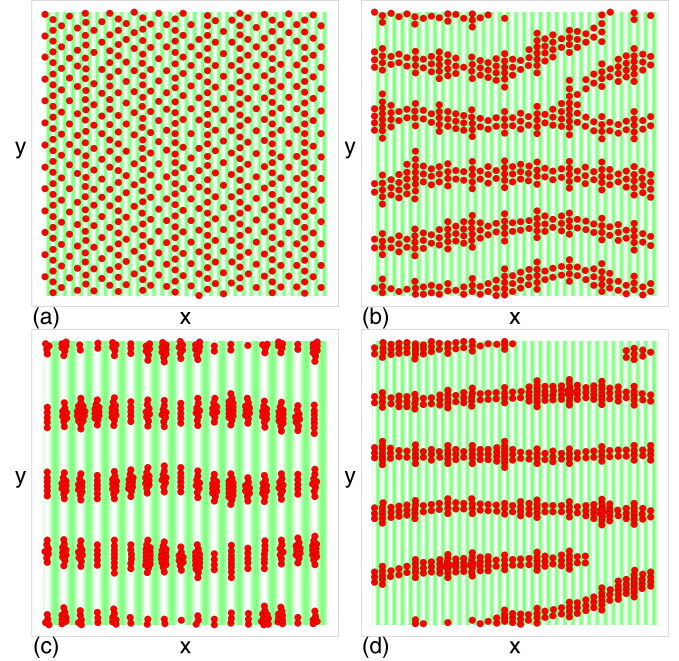

FIG. 14. Particle positions (red circles) and substrate potential (green shading) showing pinned configurations at $F_D = 0$ and $\rho = 0.44$. (a) A distorted crystal at $N_p = 35$, $F_p = 2.5$, and $B = 1.6$. (b) A pinned stripe aligned with the x direction at $N_p = 35$, $F_p = 2.5$, and $B = 2.15$. (c) A pinned modulated stripe aligned with the x direction at $N_p = 17$, $F_p = 3.0$, and $B = 2.75$. (d) A stripelike structure at $N_p = 35$, $F_p = 1.5$, and $B = 2.75$.

the stripe structures. The number of bubbles grows at later times, as shown in Figs. 15(b) and 15(c), and at long times all of the particles are contained by moving bubbles as in Fig. 15(d).

VI. VARIED FILLING

We next consider the effect of holding B, the substrate strength, and the substrate lattice constant fixed while varying the particle density ρ. In Fig. 16, we plot F_c/F_p versus ρ for samples with $F_p = 1.0$ and $N_p = 8.0$ at $B = 2.15$ in the stripe state, $B = 2.75$ in the bubble state, and $B = 1.0$ in the anisotropic crystal state. The stripe state has the highest depinning threshold across the entire range of ρ and shows some plateaus with $F_c/F_p = 1.0$ for $\rho < 0.1$, $F_c/F_p \approx 0.75$ for $0.25 < \rho < 0.5$, $F_c/F_p = 0.47$ for $0.55 < \rho < 0.85$, and a decrease in F_c/F_p at higher values of ρ. These plateaus correspond to stripes that are composed of different numbers of particles per row. In Fig. 17(a) we plot the pinned particle configurations for $B = 2.15$ at $\rho = 0.093$, where $F_c/F_p = 1.0$. Here the system forms a stripelike bubble state where each bubble is only a single particle wide and the disordered bubbles are arranged in a rough lattice configuration. Figure 17(b) shows the pinned configuration at $\rho = 0.262$ on the second plateau in F_c/F_p, where a continuous stripe structure appears in which some regions of the stripe are two particles wide. It is the regions of greater width that depin first. In general, the second plateau in F_c/F_p for the $B = 2.15$ system corresponds to values of ρ for which portions of the stripe are two particles
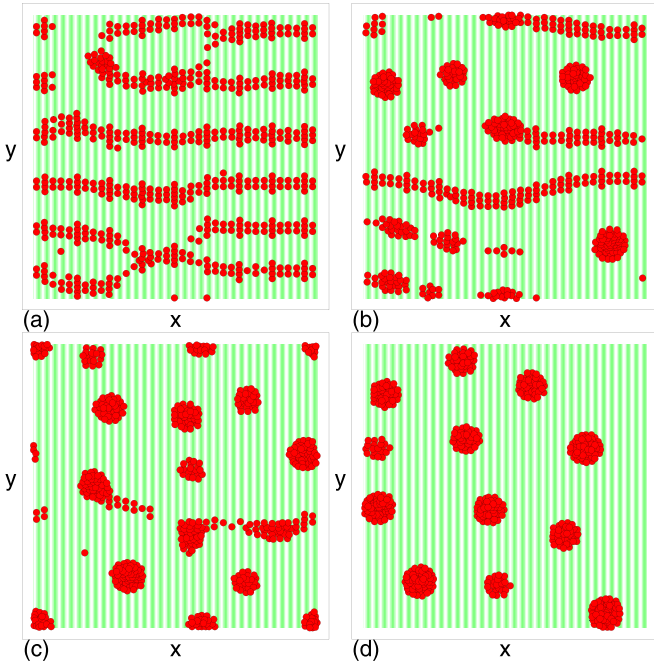
FIG. 15. Particle positions (red circles) and substrate potential (green shading) showing the time evolution of the pinned stripe into a moving bubble for $F_p = 3.0$, $B = 2.75$, $N_p = 35$, $\rho = 0.44$, and $F_D = 2.0$. (a) At early time, nascent bubbles begin translating along the stripe structures and collecting additional particles. (b) At early intermediate time, more of the pinned stripe particles become incorporated into the moving bubbles. (c) At late intermediate time, very few of the particles are still in pinned stripe structures. (d) At late time, all of the particles have joined moving bubbles.

wide. On the third plateau in F_c/F_p, as shown in Fig. 17(c) at $\rho = 0.67$, portions of the stripes are three particles wide. Figure 17(d) shows the pinned stripe configuration at $\rho = 0.938$, where the stripes now have a width of four particles. In general, we expect that there should be a series of plateaus
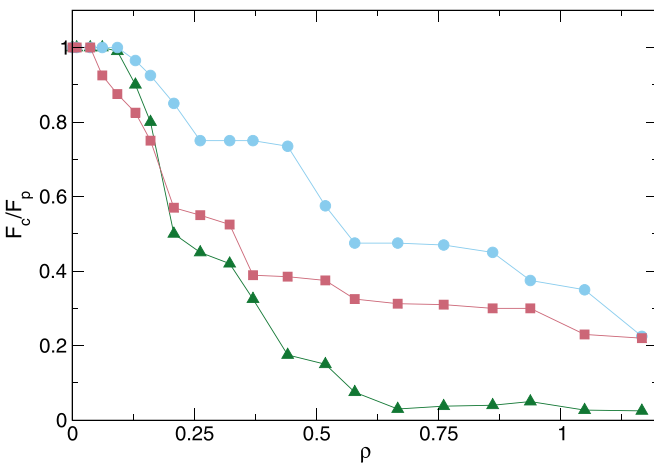

FIG. 16. The critical depinning force F_c/F_p vs particle density ρ for a system with $F_p = 1.0$ and $N_p = 8$ at $B = 2.15$ (stripes, blue circles), $B = 2.75$ (bubbles, red squares), and $B = 1.0$ (anisotropic crystal, green triangles).
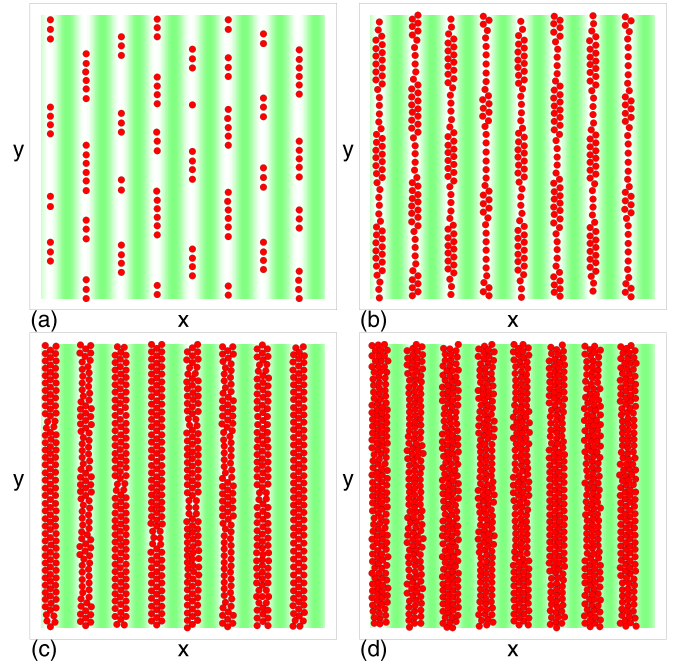

FIG. 17. Particle positions (red circles) and substrate potential (green shading) showing the pinned particle configurations for the system from Fig. 16 with $F_p = 1.0$, $N_p = 8$, and $B = 2.15$ in the stripe state at (a) $\rho = 0.093$, (b) $\rho = 0.262$, (c) $\rho = 0.67$, and (d) $\rho = 0.938$.

whenever N rows of particles can fit inside one of the substrate troughs.

In Fig. 18(a), we show the pinned particle configurations for the system from Fig. 16 in the $B = 1.0$ anisotropic crystal state at $\rho = 0.093$, where the particles form a rectangular array. Here triangular ordering is suppressed by the attractive interaction term; if the particle interactions were purely repulsive, then the particles would try to move as far away from each other as possible and would adopt a triangular configuration, but the attractive term causes square or rectangular configurations to be favored. Figure 18(b) shows the same system at $\rho = 0.262$, where stripes containing two rows of particles have formed. The pattern is more zigzag in nature compared to the $B = 2.15$ system, and there are no regions where the stripes are strictly 1D like. At $\rho = 0.518$ in Fig. 18(c), there are now three rows of particles in each substrate minimum. For the even higher density of $\rho = 0.67$, there is not enough space in the substrate minima to accommodate all of the particles, so the system becomes partially disordered and the depinning threshold drops considerably.

Figure 19(a) shows the particle configurations in the pinned bubble state for the system from Fig. 16 at $B = 2.75$ and $\rho = 0.093$, where a series of small bubbles appear. For this filling, the depinning threshold is smaller than in the stripe and anisotropic crystal states, where the particle arrangements were strictly 1D. At $\rho = 0.208$ in Fig. 19(b), the depinning threshold has dropped onto the next plateau, and the bubbles have a width of three particles. On the next plateau of the depinning threshold, illustrated in Fig. 19(c) at $\rho = 0.37$, the bubbles are much larger. Finally, for $\rho = 0.76$ in Fig. 19(d), there are even larger bubbles.
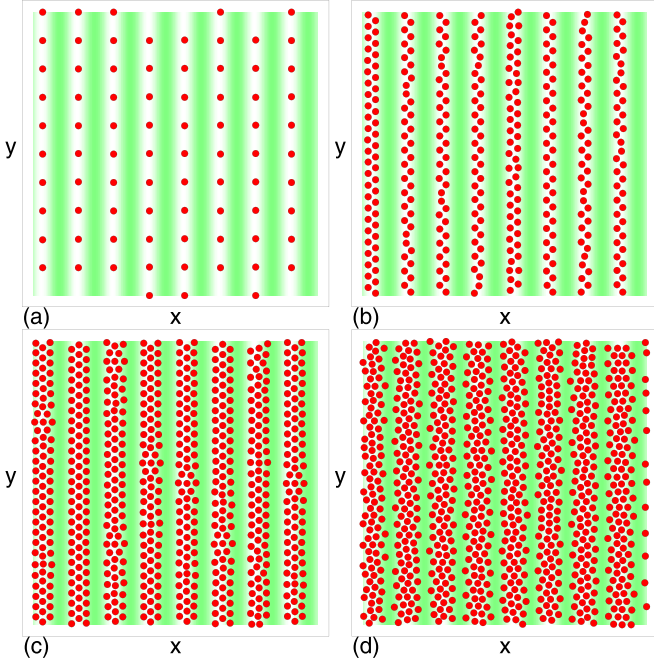
FIG. 18. Particle positions (red circles) and substrate potential (green shading) showing the pinned anisotropic crystal system from Fig. 16 with $F_p = 1.0$, $N_p = 8$, and $B = 1.0$ at (a) $\rho = 0.093$, (b) $\rho = 0.262$, (c) $\rho = 0.518$, and (d) $\rho = 0.67$.

In Figs. 20(a) and 20(b) we plot $\langle V \rangle$ and $d\langle V \rangle/dF_D$ versus F_D for the stripe system from Fig. 16 at $B = 2.15$ and $\rho = 0.093$. The depinning has the character of a single-particle process, and the system transitions from a pinned 1D bubble
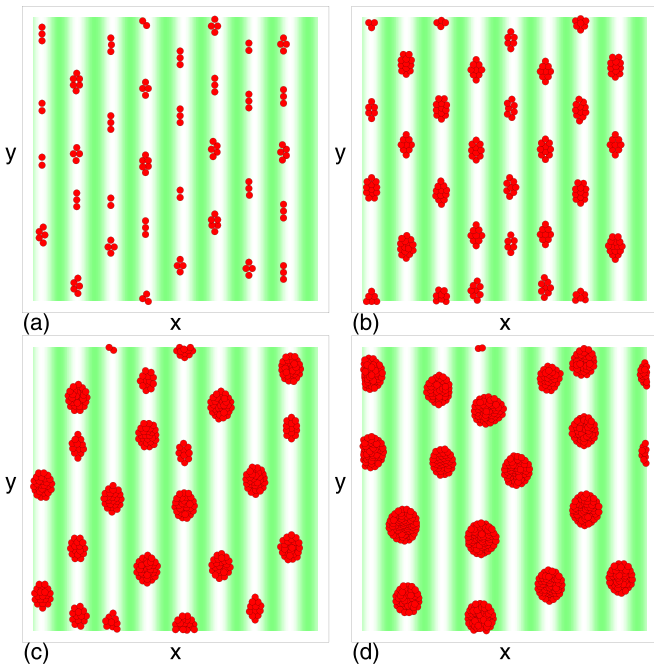

FIG. 19. Particle positions (red circles) and substrate potential (green shading) showing the pinned particle configurations for the $B = 2.75$ bubble-forming system from Fig. 16 with $F_p = 1.0$ and $N_p = 8$. (a) $\rho = 0.093$. (b) $\rho = 0.208$. (c) $\rho = 0.37$. (d) $\rho = 0.76$.
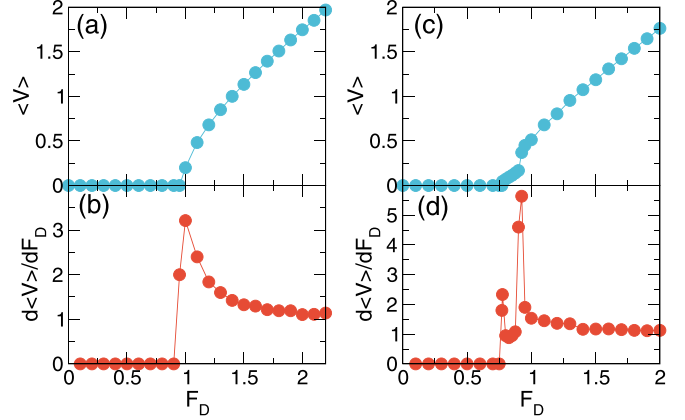

FIG. 20. [(a) and (c)]$\langle V \rangle$ vs F_D and [(b) and (d)] $d\langle V \rangle/dF_D$ vs F_D for the system from Fig. 16 with $F_p = 1.0$, $N_p = 8$, and $B = 2.15$. [(a) and (b)] $\rho = 0.093$. [(c) and (d)] $\rho = 0.26$, where there is a two step depinning process.

state to a moving dilute bubble phase. Here the depinning threshold falls slightly below $F_D/F_p = 1.0$. At these low densities, there are not enough particles present to permit a stripe phase to form, but there are still some bubblelike features in the moving state. Figure 21(a) illustrates the moving clump phase for the system in Fig. 20(a) at $F_D = 1.5$. The plots of $\langle V \rangle$ and $d\langle V \rangle/dF_D$ versus F_D in Figs. 20(b) and 20(c) for a sample with $B = 2.15$ and $\rho = 0.26$ indicate that there is a
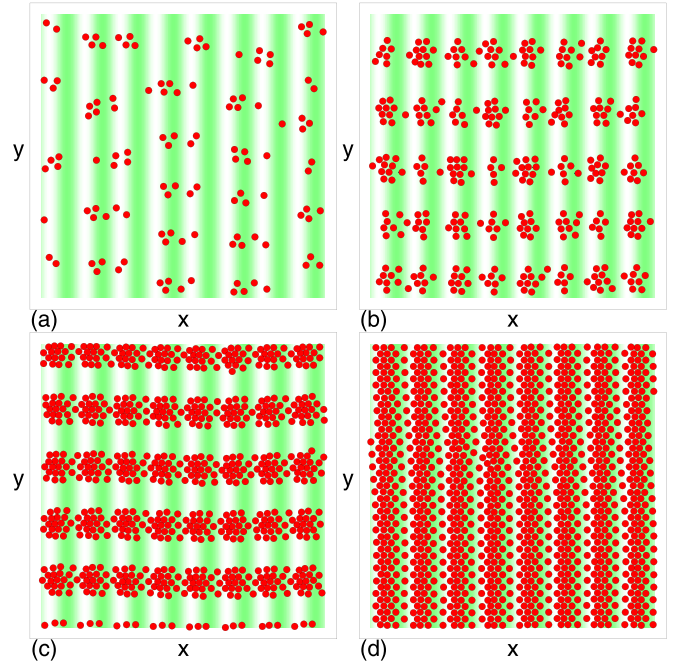

FIG. 21. Particle positions (red circles) and substrate potential (green shading) in a series of moving states at $F_D = 1.5$ in samples with $F_p = 1.0$, $N_p = 8$, and $B = 2.15$. (a) The moving clump phase for the system from Figs. 20(a) and 20(b) with $\rho = 0.093$. (b) The moving stripe phase for the system in Figs. 20(c) and 20(d) with $\rho = 0.26$. (c) The moving stripe state at $\rho = 0.578$ for the system in Figs. 22(a) and 22(b) with $\rho = 0.578$. (d) The moving modulated solid at $\rho = 0.938$ for the system in Figs. 22(c) and 22(d).
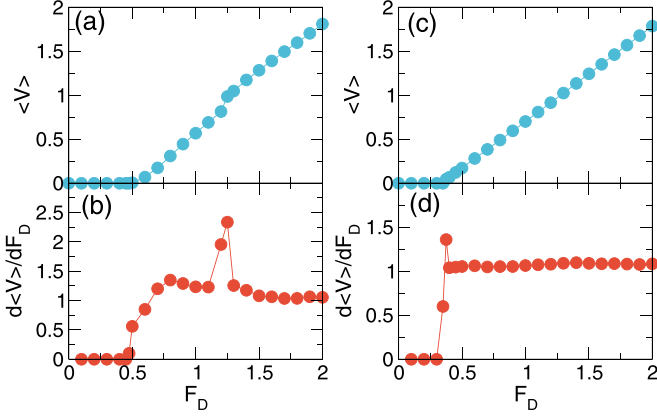
FIG. 22. [(a) and (b)] $\langle V \rangle$ vs F_D and [(c) and (d)] $d\langle V \rangle/dF_D$ vs F_D for the system from Fig. 16 with $F_p = 1.0$, $N_p = 8$, and $B = 2.15$. [(a) and (b)] $\rho = 0.578$. [(c) and (d)] $\rho = 0.938$, where there is a single elastic depinning process.

two-step depinning process accompanied by a double peak feature in the differential velocity-force curve. The system first depins into a soliton motion state in which the solitons translate through the regions containing two rows of particles. At higher drives, all of the particles depin and the system forms a moving stripe phase, as shown in Fig. 21(b) at $F_D = 1.5$.

In Figs. 22(a) and 22(b) we plot $\langle V \rangle$ and $d\langle V \rangle/dF_D$ versus F_D for the system from Fig. 20 with $B = 2.15$ at $\rho = 0.578$. Here we observe a soliton depinning process, a second depinning transition into a disordered flow state, and a dynamical reordering transition into a moving stripe state, visible as a peak in the differential mobility near $F_D = 1.25$. Figure 21(c) shows the particle configuration in the moving stripe state at $F_D = 1.5$ for $\rho = 0.578$, where each stripe has a width of five particles. The plots of $\langle V \rangle$ and $d\langle V \rangle/dF_D$ in Figs. 22(c) and 22(d) for the same sample at $\rho = 0.938$ exhibit a single peak in the differential mobility produced when the system depins elastically from a modulated solid to a moving modulated solid. Here the stripes do not reorient into the direction of driving and remain parallel to the substrate troughs. Figure 21(d) illustrates the moving modulated solid state for $F_D = 1.5$ at $\rho = 0.938$.

From the features in the transport curves and the particle configurations, in Fig. 23 we construct a dynamic phase diagram as a function of F_D vs ρ for the system with $B = 2.15$, $F_p = 1.0$, and $N_p = 8$ where we highlight the pinned regime, moving So state, disordered motion (D) phase, MS state, MB phase, and moving modulated crystal. The system cannot form a moving stripe when $\rho < 0.25$ and instead enters the moving bubble phase. The moving stripe phase occurs in a window of density ranging from $0.25 \leqslant \rho < 0.8$. In a portion of this density window, we find that the system first passes through a moving modulated solid state before transitioning to the moving stripe configuration.

VII. REENTRANT PINNING PHASES

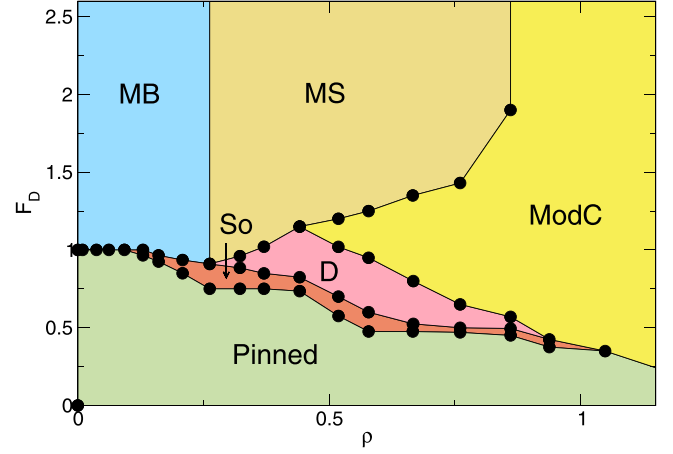We have demonstrated above that the stripe state is the most strongly pinned phase; however, for large B the smaller

FIG. 23. Dynamic phase diagram as a function of F_D vs ρ for a system with $B = 2.15$, $F_p = 1.0$, and $N_p = 8$. The distinct pinned states are not resolved and are marked as a Pinned region. The moving states are soliton motion (So), disordered (D) flow, moving bubble (MB), moving stripe (MS), and moving modulated crystal (ModC).

bubbles are also very strongly pinned, suggesting that it should be possible to observe *multiple* reentrant pinning effects under the right conditions. We consider a sample with $N_p = 8$ and strong pinning of $F_p = 5.0$ under a constant driving force of $F_D = 4.0$. In Fig. 24, we plot $\langle V \rangle$ versus B for this system at $\rho = 0.129$, 0.208, 0.262, 0.322, 0.44, 0.67, and 1.16. For $\rho = 0.129$, the system is pinned for all values of B, while for $\rho = 0.262$, 0.322, and 0.44, the system is initially flowing at very small B, enters a pinned stripe state near
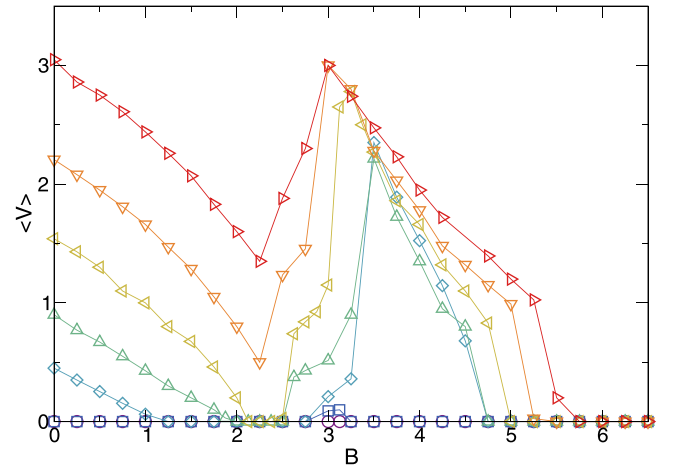

FIG. 24. $\langle V \rangle$ vs B for a system with $N_p = 8$, $F_p = 5.0$, and $F_D = 4.0$ for $\rho = 0.129$ (violet circles), 0.208 (dark blue squares), 0.262 (light blue diamonds), 0.322 (green up triangles), 0.44 (yellow left triangles), 0.67 (orange down triangles), and 1.16 (red right triangles). Two distinct pinned phases appear. Near $B = 2.15$ is the pinned stripe regime, and in the region above $B = 4.75$ is the pinned small bubble regime. At very small B is the weakly pinned crystalline state, and there is a window of large bubble states in between the stripe and small bubble states that is also weakly pinned. As a result, there can be a doubly reentrant pinned state as a function of increasing B.

$B = 2.15$, and develops a finite velocity again in the bubble phase for $B > 2.3$. There is a local maximum in the velocity near $B = 3.0$; however, as B increases further, the bubbles shrink in size and become pinned again for sufficiently large B, reaching a second reentrant pinned state. For $\rho > 0.44$, there is a dip in $\langle V \rangle$ near $B = 2.15$ in the stripe phase but the system does not become reentrantly pinned; this is followed by a local maximum in $\langle V \rangle$ in the large bubble phase and a reentrant pinning of the small bubble state for large B. Going to large values of B has an effect on the transport that is similar to going to low particle density, since the increase of B causes the average spacing between adjacent bubbles to get larger as the bubble radius becomes smaller. In particular, the depinning threshold approaches $F_c/F_p = 1.0$ for both large B and small ρ. In Fig. 24, we have fixed $F_D/F_p = 0.8$, so once F_c/F_p exceeds this value either by decreasing ρ or increasing B in the small bubble phase, the velocity drops to zero and a pinned state emerges.

VIII. DISCUSSION

The results we obtain with the present model can be compared to those found in previous studies of particles on 2D periodic substrates. In general, in the previous works, the interactions between particles were purely repulsive, such as for superconducting vortices, charged particles, screened Coulomb interactions, or hard disks. In purely repulsive systems for fixed density, the critical depinning force decreases monotonically when the interaction strength of the particles increases, and varies as a function of particle density depending on whether the particle configuration is commensurate or incommensurate with the substrate. In a commensurate state, the particles can form a triangular lattice that fits into the substrate in such a way that no kinks are present. In this case, the system behaves almost like a single particle, so that the depinning threshold is maximized and becomes independent of the particle-particle interaction strength. Commensurate conditions only occur for certain fillings or densities, as studied for superconducting vortices [52,54] and colloidal particles [47–49,64]. For incommensurate conditions, the depinning threshold monotonically decreases with increasing particle-particle interaction strength since the particles form an ever-stiffer lattice that couples less and less well to the substrate [52,54].

In our pattern-forming system, we find a nonmonotonic change in the depinning force that is correlated with the formation of different patterns. When the strength B of the attractive component of the particle-particle interaction is increased, there is a peak in the depinning threshold when the system forms a stripe state that can align with the substrate. The depinning threshold decreases with increasing attraction in the crystal phase because increasing the attraction effectively lowers the strength of the repulsion, softening the lattice and allowing it to interact more strongly with the substrate. For particles with purely repulsive interactions, similar lattice softening occurs when the particle-particle interaction strength is decreased. At the onset of the bubble phase, we find that the depinning threshold initially drops with increasing B because the bubbles are unable to fit inside the potential

wells in the same way as the stripe state could; however, for higher attraction values the depinning threshold increases with increasing B because the bubbles begin to shrink and the behavior of the system becomes similar to that of purely repulsive point particles. We observe two important effects that are not found for purely repulsive particles: changes in the morphology, and the impact of the finite width of the quasi-point-like particles. These effects produce new types of dynamics that do not appear for purely repulsive particles, including the hopping of individual particles from one stripe to another or from one bubble to another. Additionally, the stripes have an orientational degree of freedom, so that we can observe a transition from stripes that are parallel to the substrate troughs to stripes that are perpendicular to the substrate troughs as a function of drive. The internal degrees of freedom of the stripes and bubbles also make it possible for distinct types of plastic flow phases to arise that are absent in the purely repulsive particle limit.

Pattern-forming systems on a 1D substrate exhibit a variety of additional effects that would be interesting to explore in future studies, such as thermal or creep effects, where it would be possible to compare stripe creep to bubble or anisotropic crystal creep, as well as differences between creep in the elastic depinning regime and creep in the plastic depinning regime. Several previous studies of particles with purely repulsive interactions coupled to a 1D periodic substrate demonstrated reentrant melting or smectic phases as a function of increasing substrate strength or filling [44,45,47,64]. In this work we considered purely dc driving, but if ac driving were applied, then we would expect to observe Shapiro step phenomena [39], and it would be possible to explore whether the Shapiro steps are enhanced in the stripe phase compared to the bubble phase. Another direction would be to consider a 2D substrate that could break apart the stripes or lock the flow of the stripe phase into particular directions. Other interesting effects to explore include the effect of adding a small amount of random point disorder or a random shift to the substrate. Our results should be general to the broader class of stripe or bubble-forming systems, including those that have different kinds of interactions, such as a purely repulsive interaction potential with two length scales.

The closest experimental realization of the system we consider here could be achieved by adding a 1D substrate to a 2D electron gas, which forms crystal, stripe, and bubble states as a function of an applied magnetic field. Here the pinning resonance or transport curves could be measured under changing magnetic field as the system is tuned from the stripe to the bubble phase. Another possibility is to use low-κ superconductors, which can form bubble and stripe states, coupled to periodic one-dimensional substrates similar to those employed in previous studies [52]. For soft-matter systems, one could study colloidal particles on 1D substrates [44,45,47,64] where the colloids have an additional longer-range repulsion and short-range attraction. Recently, there has been an experimental realization of magnetic particles on an interface that interact via a combination of longer-range repulsion and short-range attraction, where crystal, stripe, and bubble patterns can form [65]. The dynamic phases that we observe could be produced by placing such a system on a periodic 1D substrate and subjecting it to a driving force.

IX. SUMMARY

We have numerically investigated the pinning and dynamics of a two-dimensional pattern-forming system consisting of particles with long-range repulsion and short-range attraction interacting with a periodic one-dimensional substrate. In the absence of a substrate, this system forms a crystal for very low attraction strength, an anisotropic crystal at weak attraction strength, a stripe lattice for intermediate attraction strength, and a bubble lattice for strong attraction. When a one-dimensional substrate is added to the sample, we find that the stripe state is the most strongly pinned overall and is particularly strongly pinned whenever the stripes are commensurate with the substrate spacing and can align with the substrate minima. In the bubble phase, when the bubbles are large they do not fit into a single substrate minimum and are weakly pinned; however, small bubbles that can fit inside the substrate minima are strongly pinned. The anisotropic crystal and stripe states can depin plastically either via the motion of solitons or directly into a disordered flow phase, and at higher drives, the system can dynamically order into a moving crystal state or moving stripes that have rotated with respect to the pinned state and are aligned with the driving direction. We show that this system exhibits a wide variety of dynamical phases, and that transitions between the different phases are observable as multiple steps or peaks in the velocity-force curves and differential velocity curves. For small substrate lattice constants, the stripe and bubble phases are replaced by pinned modulated stripe phases with stripes that are perpendicular to the substrate troughs, in contrast to the case of large substrate spacing where the stripes are aligned with the substrate troughs. We map out the dynamic phases as a function of substrate strength, attraction strength, density, and driving force. At high densities, the stripes remain oriented with the substrate trough direction and not with the driving direction even in the moving state. Our results are relevant for a wide variety of similar pattern-forming systems in both soft- and hard-matter systems that are coupled to a periodic one-dimensional substrate.

[1] M. Seul and D. Andelman, Domain shapes and patterns—The phenomenology of modulated phases, Science **267**, 476 (1995).

[2] A. D. Stoycheva and S. J. Singer, Stripe melting in a two-dimensional system with competing interactions, Phys. Rev. Lett. **84**, 4657 (2000).

[3] C. Reichhardt, C. J. Olson, I. Martin, and A. R. Bishop, Depinning and dynamics of systems with competing interactions in quenched disorder, Europhys. Lett. **61**, 221 (2003).

[4] C. J. O. Reichhardt, C. Reichhardt, I. Martin, and A. R. Bishop, Dynamics and melting of stripes, crystals, and bubbles with quenched disorder, Physica D **193**, 303 (2004).

[5] S. Mossa, F. Sciortino, P. Tartaglia, and E. Zaccarelli, Ground-state clusters for short-range attractive and long-range repulsive potentials, Langmuir **20**, 10756 (2004).

[6] F. Sciortino, S. Mossa, E. Zaccarelli, and P. Tartaglia, Equilibrium cluster phases and low-density arrested disordered states: The role of short-range attraction and long-range repulsion, Phys. Rev. Lett. **93**, 055701 (2004).

[7] K. Nelissen, B. Partoens, and F. M. Peeters, Bubble, stripe, and ring phases in a two-dimensional cluster with competing interactions, Phys. Rev. E **71**, 066204 (2005).

[8] Y. H. Liu, L. Y. Chew, and M. Y. Yu, Self-assembly of complex structures in a two-dimensional system with competing interaction forces, Phys. Rev. E **78**, 066405 (2008).

[9] C. J. O. Reichhardt, C. Reichhardt, and A. R. Bishop, Structural transitions, melting, and intermediate phases for stripe- and clump-forming systems, Phys. Rev. E **82**, 041502 (2010).

[10] D. McDermott, C. J. O. Reichhardt, and C. Reichhardt, Structural transitions and hysteresis in clump- and stripe-forming systems under dynamic compression, Soft Matter **12**, 9549 (2016).

[11] Y. Liu and Y. Xi, Colloidal systems with a short-range attraction and long-range repulsion: phase diagrams, structures, and dynamics, Curr. Opin. Colloid Interf. Sci. **39**, 123 (2019).

[12] X. B. Xu, T. Tang, Z. H. Wang, X. N. Xu, G. Y. Fang, and M. Gu, Nonequilibrium pattern formation in circularly confined two-dimensional systems with competing interactions, Phys. Rev. E **103**, 012604 (2021).

[13] E. A. Jagla, Phase behavior of a system of particles with core collapse, Phys. Rev. E **58**, 1478 (1998).

[14] G. Malescio and G. Pellicane, Stripe phases from isotropic repulsive interactions, Nat. Mater. **2**, 97 (2003).

[15] M. A. Glaser, G. M. Grason, R. D. Kamien, A. Kosmrlj, C. D. Santangelo, and P. Ziherl, Soft spheres make more mesophases, Europhys. Lett. **78**, 46004 (2007).

[16] L. Q. Costa Campos, S. W. S. Apolinario, and H. Löwen, Structural ordering of trapped colloids with competing interactions, Phys. Rev. E **88**, 042313 (2013).

[17] M. M. Fogler, A. A. Koulakov, and B. I. Shklovskii, Ground state of a two-dimensional electron liquid in a weak magnetic field, Phys. Rev. B **54**, 1853 (1996).

[18] R. Moessner and J. T. Chalker, Exact results for interacting electrons in high Landau levels, Phys. Rev. B **54**, 5006 (1996).

[19] K. B. Cooper, M. P. Lilly, J. P. Eisenstein, L. N. Pfeiffer, and K. W. West, Insulating phases of two-dimensional electrons in high Landau levels: Observation of sharp thresholds to conduction, Phys. Rev. B **60**, R11285 (1999).

[20] W. Pan, R. R. Du, H. L. Stormer, D. C. Tsui, L. N. Pfeiffer, K. W. Baldwin, and K. W. West, Strongly anisotropic electronic transport at landau level filling factor $\nu = 9/2$ and $\nu = 5/2$ under a tilted magnetic field, Phys. Rev. Lett. **83**, 820 (1999).

[21] E. Fradkin and S. A. Kivelson, Liquid-crystal phases of quantum Hall systems, Phys. Rev. B **59**, 8065 (1999).

[22] J. Göres, G. Gamez, J. H. Smet, L. Pfeiffer, K. West, A. Yacoby, V. Umansky, and K. von Klitzing, Current-induced anisotropy and reordering of the electron liquid-crystal phases in a two-dimensional electron system, Phys. Rev. Lett. **99**, 246402 (2007).

[23] H. Zhu, G. Sambandamurthy, L. W. Engel, D. C. Tsui, L. N. Pfeiffer, and K. W. West, Pinning mode resonances of 2D electron stripe phases: Effect of an in-plane magnetic field, Phys. Rev. Lett. **102**, 136804 (2009).

[24] B. Friess, V. Umansky, K. von Klitzing, and J. H. Smet, Current flow in the bubble and stripe phases, Phys. Rev. Lett. **120**, 137603 (2018).

[25] V. Shingla, H. Huang, A. Kumar, L. N. Pfeiffer, K. W. West, K. W. Baldwin, and G. A. Csáthy, A highly correlated topological bubble phase of composite fermions, Nat. Phys. **19**, 689 (2023).

[26] X. B. Xu, H. Fangohr, S. Y. Ding, F. Zhou, X. N. Xu, Z. H. Wang, M. Gu, D. Q. Shi, and S. X. Dou, Phase diagram of vortex matter of type-II superconductors, Phys. Rev. B **83**, 014501 (2011).

[27] L. Komendová, M. V. Milošević, and F. M. Peeters, Soft vortex matter in a type-I/type-II superconducting bilayer, Phys. Rev. B **88**, 094515 (2013).

[28] C. N. Varney, K. A. H. Sellin, Q.-Z. Wang, H. Fangohr, and E. Babaev, Hierarchical structure foramtion in layered superconducting systems with multi-scale inter-vortex interactions, J. Phys.: Condens. Matter **25**, 415702 (2013).

[29] K. A. H. Sellin and E. Babaev, Stripe, gossamer, and glassy phases in systems with strong nonpairwise interactions, Phys. Rev. E **88**, 042305 (2013).

[30] X. S. Brems, S. Mühlbauer, W. Y. Córdoba-Camacho, A. A. Shanenko, A. Vagov, J. A. Aguiar, and R. Cubitt, Current-induced self-organisation of mixed superconducting states, Supercond. Sci. Technol. **35**, 035003 (2022).

[31] C. Reichhardt, C. J. O. Reichhardt, and M. V. Milošević, Statics and dynamics of skyrmions interacting with disorder and nanostructures, Rev. Mod. Phys. **94**, 035005 (2022).

[32] J. M. Tranquada, B. J. Sterlieb, J. D. Axe, Y. Nakamura, and S. Uchida, Evidence for stripe correlations of spins and holes in copper-oxide superconductors, Nature (London) **375**, 561 (1995).

[33] C. J. O. Reichhardt, C. Reichhardt, and A. R. Bishop, Fibrillar templates and soft phases in systems with short-range dipolar and long-range interactions, Phys. Rev. Lett. **92**, 016801 (2004).

[34] T. Mertelj, V. V. Kabanov, and D. Mihailovic, Charged particles on a two-dimensional lattice subject to anisotropic Jahn-Teller interactions, Phys. Rev. Lett. **94**, 147003 (2005).

[35] P. G. Baity, T. Sasagawa, and D. Popović, Collective dynamics and strong pinning near the onset of charge order in La$_{1.48}$ Nd$_{0.4}$ Sr$_{0.12}$ CuO$_4$, Phys. Rev. Lett. **120**, 156602 (2018).

[36] S. Mahmoudian, L. Rademaker, A. Ralko, S. Fratini, and V. Dobrosavljević, Glassy dynamics in geometrically frustrated Coulomb liquids without disorder, Phys. Rev. Lett. **115**, 025701 (2015).

[37] C. Reichhardt, C. J. O. Reichhardt, I. Martin, and A. R. Bishop, Dynamical ordering of driven stripe phases in quenched disorder, Phys. Rev. Lett. **90**, 026401 (2003).

[38] H. J. Zhao, V. R. Misko, and F. M. Peeters, Dynamics of self-organized driven particles with competing range interaction, Phys. Rev. E **88**, 022914 (2013).

[39] C. Reichhardt and C. J. O. Reichhardt, Depinning and nonequilibrium dynamic phases of particle assemblies driven over random and ordered substrates: A review, Rep. Prog. Phys. **80**, 026501 (2017).

[40] K. Bennaceur, C. Lupien, B. Reulet, G. Gervais, L. N. Pfeiffer, and K. W. West, Competing charge density waves probed by nonlinear transport and noise in the second and third Landau levels, Phys. Rev. Lett. **120**, 136801 (2018).

[41] J. Sun, J. Niu, Y. Li, Y. Liu, L. N. Pfeiffer, K. W. West, P. Wang, and X. Lin, Dynamic ordering transitions in charged solid, Fund. Res. **2**, 178 (2022).

[42] Q. Qian, J. Nakamura, S. Fallahi, G. C. Gardner, and M. J. Manfra, Possible nematic to smectic phase transition in a two-dimensional electron gas at half-filling, Nat. Commun. **8**, 1536 (2017).

[43] P. T. Madathil, K. A. Villegas Rosales, Y. J. Chung, K. W. West, K. W. Baldwin, L. N. Pfeiffer, L. W. Engel, and M. Shayegan, Moving crystal phases of a quantum Wigner solid in an ultra-high-quality 2D electron system, Phys. Rev. Lett. **131**, 236501 (2023).

[44] A. Chowdhury, B. J. Ackerson, and N. A. Clark, Laser-induced freezing, Phys. Rev. Lett. **55**, 833 (1985).

[45] J. Chakrabarti, H. R. Krishnamurthy, A. K. Sood, and S. Sengupta, Reentrant melting in laser field modulated colloidal suspensions, Phys. Rev. Lett. **75**, 2232 (1995).

[46] K. Harada, O. Kamimura, H. Kasai, T. Matsuda, A. Tonomura, and V. V. Moshchalkov, Direct observation of vortex dynamics in superconducting films with regular arrays of defects, Science **274**, 1167 (1996).

[47] E. Frey, D. R. Nelson, and L. Radzihovsky, Light-induced melting of colloidal crystals in two dimensions, Phys. Rev. Lett. **83**, 2977 (1999).

[48] Q.-H. Wei, C. Bechinger, D. Rudhardt, and P. Leiderer, Experimental study of laser-induced melting in two-dimensional colloids, Phys. Rev. Lett. **81**, 2606 (1998).

[49] C. Bechinger, M. Brunner, and P. Leiderer, Phase behavior of two-dimensional colloidal systems in the presence of periodic light fields, Phys. Rev. Lett. **86**, 930 (2001).

[50] C. Reichhardt and C. J. Olson, Novel colloidal crystalline states on two-dimensional periodic substrates, Phys. Rev. Lett. **88**, 248301 (2002).

[51] M. Brunner and C. Bechinger, Phase behavior of colloidal molecular crystals on triangular light lattices, Phys. Rev. Lett. **88**, 248302 (2002).

[52] P. Martinoli, Static and dynamic interaction of superconducting vortices with a periodic pinning potential, Phys. Rev. B **17**, 1175 (1978).

[53] C. Reichhardt, C. J. Olson, and F. Nori, Dynamic phases of vortices in superconductors with periodic pinning, Phys. Rev. Lett. **78**, 2648 (1997).

[54] Q. Le Thien, D. McDermott, C. J. O. Reichhardt, and C. Reichhardt, Orientational ordering, buckling, and dynamic transitions for vortices interacting with a periodic quasi-one-dimensional substrate, Phys. Rev. B **93**, 014504 (2016).

[55] G. R. Berdiyorov, M. V. Milošević, and F. M. Peeters, Novel commensurability effects in superconducting films with antidot arrays, Phys. Rev. Lett. **96**, 207001 (2006).

[56] D. McDermott, C. J. O. Reichhardt, and C. Reichhardt, Stripe systems with competing interactions on quasi-one dimensional periodic substrates, Soft Matter **10**, 6332 (2014).

[57] C. Reichhardt and C. J. O. Reichhardt, Sliding dynamics for bubble phases on periodic modulated substrates, Phys. Rev. Res. **6**, 023116 (2024).

[58] S. Bhattacharya and M. J. Higgins, Dynamics of a disordered flux line lattice, Phys. Rev. Lett. **70**, 2617 (1993).

[59] K. Moon, R. T. Scalettar, and G. T. Zimányi, Dynamical phases of driven vortex systems, Phys. Rev. Lett. **77**, 2778 (1996).

[60] L. Balents, M. C. Marchetti, and L. Radzihovsky, Nonequilibrium steady states of driven periodic media, Phys. Rev. B **57**, 7705 (1998).

[61] C. J. Olson, C. Reichhardt, and F. Nori, Nonequilibrium dynamic phase diagram for vortex lattices, Phys. Rev. Lett. **81**, 3757 (1998).

[62] F. Pardo, F. de la Cruz, P. L. Gammel, E. Bucher, and D. J. Bishop, Observation of smectic and moving-Bragg-glass phases in flowing vortex lattices, Nature (London) **396**, 348 (1998).

[63] C. Reichhardt, D. Ray, and C. J. O. Reichhardt, Collective transport properties of driven skyrmions with random disorder, Phys. Rev. Lett. **114**, 217202 (2015).

[64] L. Radzihovsky, E. Frey, and D. R. Nelson, Novel phases and reentrant melting of two-dimensional colloidal crystals, Phys. Rev. E **63**, 031503 (2001).

[65] A. Hooshanginejad, J.-W. Barotta, V. Spradlin, G. Pucci, R. Hunt, and D. M. Harris, Mermaid cereal: Interactions and pattern formation in a macroscopic magnetocapillary SALR system, arXiv:2403.01097